Effect of resonant coherent excitation on the electronic stopping of slow channeled ions

Chang-Kai Li,[1,2] Sheng Liu,[1,2,*] Qiang Cao,[1] Feng Wang,[3] Xiao-ping OuYang,[4] and Feng-Shou Zhang[4,5,6,†]

[1]*The Institude of Technological Science, Wuhan University, Wuhan 430072, China*

[2]*School of Power and Mechanical Engineering, Wuhan University, Wuhan 430072, China*

[3]*School of Physics, Beijing Institute of Technology, Beijing 100081, China*

[4]*The Key Laboratory of Beam Technology and Material Modification of Ministry of Education, College of Nuclear Science and Technology, Beijing Normal University, Beijing 100875, China*

[5]*Beijing Radiation Center, Beijing 100875, China*

[6]*Center of Theoretical Nuclear Physics, National Laboratory of Heavy Ion Accelerator of Lanzhou, Lanzhou 730000, China*

(Received 7 May 2019; revised manuscript received 2 October 2019; published 20 November 2019)

We calculated the nonlinear screening and the electronic stopping of energetic helium ions in a III-V compound semiconductor at low speeds below stopping maximum under channeling conditions. For the range of velocity considered, it is found the energy loss of the intruding ions show pronounced dependence on the electronic screening from the induced charge. Different with the prevalent scenario described by free-electron gas model that the induced charge distribution lags behind the projectile forming the so-called wake potential. We found through real-time time-dependent density functional theory that the induced charge by the channeling ion keeps oscillating back and front when channeling through the zinc-blende crystalline GaN, which is interpreted as a consequence of temporally oscillating Coulomb field arising from the periodical atomic arrangement along ion trajectory. When one of the frequencies coincides with the transition energy of the ionic charge, it would be resonantly excited by the oscillating field, which further gives rise to a depletion in electronic screening by bound electrons to the ion, resulting in odd enhanced stopping trend at narrow velocity windows.

DOI: 10.1103/PhysRevA.100.052707

I. INTRODUCTION

When ions propagate through solid matter they gradually deposit kinetic energy by electronic excitations and by collisions with lattice atoms; the energy losses per units path length are quantitatively defined as electronic stopping S_e and nuclear stopping S_n, respectively. For fast ions with velocity wildly above Thomas-Fermi speed $v_F = Z_1^{2/3} v_0$, where Z_1 is the atomic number of the projectile and v_0 the Bohr speed, the ionic charge is well stripped and the theories of Bethe and Bloch [1,2] make a sound description of the energy-loss process. For slow projectile ions with kinetic energy of several hundred keV/u and below, the projectile ion is only partially stripped, and it is surrounded by a cloud of polarized charge [3]. One must account for the perturbation introduced in the host medium by the intruding ion and the chemical aspect of the energy loss such as the effective charge [4–7] and the charge transfer [8–11] between the projectile and host atoms.

Detailed quantitative knowledge of energy dissipation processes is of central significance to understand the damage produced in materials when exposed to ion radiation, such as hydrogen ions impinging on the inner wall of a controlled thermonuclear reactor. The global stopping maximum, which is a balance between the charge state of the penetrating ion and the interaction cross sections between ion and target electrons, occurs shortly before the ion stops eventually [12]. Hence, charged particles moving with low velocity is of special significance [13]. Stopping power of slow ions with kinetic energy below and 25 keV/u($v \leqslant v_0 = c/137$) is currently a subject of intensive research. In such regime, the electronic energy loss is predominantly arising from interaction with valence electrons [14]. The simplest model that can reasonably characterize the energy loss of ions to the electronic system is that an ion moves in free-electron gas (FEG). In this formalism, Fermi and Teller [15] and consecutive studies [16,17] predicted that electronic stopping $S_e \propto v$ for a slow projectile traversing a metallic medium. The existing data tabulations [18] basically confirm this prediction.

Channeling is a limiting case that simplifies the study of electronic energy loss. Since energetic ions impinging on a surface and aligned with low-index crystallographic axes or planes can penetrate considerable distances without undergoing direct collision with a host nucleus, the vast majority of kinetic energy is essentially dissipated electronically [19]. In 1978, Datz *et al.* [20] observed resonant peaks in the probability of excitation processes for swift channeling ions with energies above 1.5 MeV/u in silver and gold crystals. Such resonances were predicted by Okorokov [21] to occur when the potential sensed by the channeling ion, periodic in time and space, stimulates electronic transitions between its core states, resulting in the presence of inner-shell vacancies on the projectile ions [22,23]. The situations for slow ions are much more complicated, since characteristic excitation energies lie within the valence band of the ion, charge transfer, and screening effect of bound charge are hence revelent. These resonant excitations are interesting electronic structure related

*Corresponding author: victor_liu63@vip.126.com

†Corresponding author: fszhang@bnu.edu.cn

aspects of channeling, which cannot be predicted within the standard framework of ions traveling through free-electron gas.

Energy loss of heavy ions in an electron gas are known to have a strong dependence on electronic screening [3], which correlates with its effective charge [24–26]. This is challenging, to what extent the charge state due to partial neutralization of the penetrating ion affects the energy loss process, which is related closely with the charge transfer dynamics. Early theoretical efforts on heavy-ion stopping date back to Bohr [27] who pointed out the importance of screening due to projectile electron in the slowing down of fission fragments. Subsequently, the role of the projectile charge and charge exchange in conjunction with stopping phenomena were discussed in detail by Bohr and Lindhard [28].

The presence of density-functional theory (DFT) allows the calculation of the energy dissipation, electron density fluctuation, induced screened potential, in a self-consistent way. Based on the FEG models, the pioneering calculations of the stopping power in this formalism were performed by Echenique, Nieminen, and Ritchie for hydrogen and helium [29], and later were extended to ions with higher charges [30]. Furthermore, beyond the FEG approximation, recent development of DFT [31–33] explicitly takes into account the effects of inhomogeneity in electron density due to the underlying lattice structure, band structure, and band gap.

In this work, we demonstrate through time-dependent density-functional theory (TDDFT) that the electronic screening by the induced charge affects the energy loss of the slow channeling helium ions, which are partially neutralized in a nontrivial manner: S_e shows a specific dependence on the charge state of the projectile. We also report a velocity-dependent charge-resonance phenomenon namely excitation of valence electrons on the channeled ion by the periodical field from an array of the atomic planes. Such work is largely inspired by the similar results reported by Mason and Race *et al.* [19,34], which are mainly achieved under the framework of tight-binding model. These modes of resonant excitation can only be activated at narrow windows when the frequencies at which the channeled ion moves from interstitial point to equivalent interstitial point, correspond to transition energies of bound states charge on the channeling ion. The charge resonance significantly affect the charge state of the projectile, which furthermore leads to counterintuitive S_e versus the velocity at narrow windows.

This paper is outlined as follows. In Sec. II, we briefly introduce the theoretical framework and the computational details. Results are presented and discussed in Sec. III, where we concentrate on the following three parts: we first discuss in detail the effect of induced charge on S_e in Sec. III A; then we demonstrate in Sec. III B a charge-resonance phenomenon induced by the periodical field from atomic planes; in the end, we make analysis of the direction-dependence of charge-resonance in Sec. III C. Conclusions are drawn in Sec. IV.

II. MODEL AND METHODS

We characterize the collision of intruding ions with the host nuclei and electrons by using the Ehrenfest coupled electron-ion dynamics [35–38]. In this model, the ions are treated as point particles, evolution of electrons are performed quantum mechanically following the time-dependent Schrödinger equation, [atomic units (a.u.) are used]

$$i\frac{\partial\Psi(x,t)}{\partial t} = \hat{H}_e(\vec{r},\vec{R}(t))\Psi(x,t), \tag{1}$$

where $\Psi(x,t)$ is the many–body electron wave function in the time domain, for which we define $x \equiv \{x_j\}_{j=1}^{N}$ (N is the number of electrons of the system), with $x_j \equiv (\vec{r}_j, \sigma_j)$, here the coordinates $\vec{r}_j$ and the spin σ_j of the jth electron are implicitly taken into account. $\hat{H}_e(\vec{r},\vec{R}(t))$ is the electronic Hamiltonian, which depends implicitly on time through its parametrization in terms of the electronic distribution $\vec{r}$ and ionic coordinates $\vec{R}(t) \equiv \{\vec{R}_1(t),\ldots,\vec{R}_M(t)\}$ (M is the number of nuclei of the system); thus, it basically consists of the kinetic energy of electrons, the electron-electron potential, and the electron-nuclei potential, which can be expressed as

$$\hat{H}_e(\vec{r},\vec{R}(t)) = -\sum_{j}^{N}\frac{1}{2}\nabla_j^2 + \sum_{i<j}\frac{1}{|\vec{r}_i-\vec{r}_j|} - \sum_{iI}\frac{Z_I}{|\vec{R}_I-\vec{r}_i|}. \tag{2}$$

The ions in turn evolve according to Newton's laws under pairwise repulsive forces and Hellmann-Feynman forces due to the electronic system

$$M_I\frac{d^2\vec{R}_I(t)}{dt^2} = -\int\Psi^*(x,t)[\nabla_I\hat{H}_e(\vec{r},\vec{R}(t))]\Psi(x,t)dx - \nabla_I\sum_{I\neq J}\frac{Z_IZ_J}{|\vec{R}_I(t)-\vec{R}_J(t)|}, \tag{3}$$

where M_I and Z_I denote the mass and charge of the Ith nuclei, respectively, and $\vec{R}_I(t)$ describes the corresponding ionic position vector.

The coupled differential Eqs. (1) and (3) define Ehrenfest coupled electron-ion dynamics. To solve Eq. (3) for the motion of the nuclei, one has to obtain knowledge of $\Psi(x,t)$, which typically leads the problem to be intractable. In view of this, we write the forces that act on each nucleus in terms of the electronic density $n(\vec{r},t)$. Consequently, Eq. (3) can be rewritten as

$$M_I\frac{d^2\vec{R}_I(t)}{dt^2} = -\int n(\vec{r},t)[\nabla_I\hat{H}_e(\vec{r},\vec{R}(t))]d\vec{r} - \nabla_I\sum_{I\neq J}\frac{Z_IZ_J}{|\vec{R}_I(t)-\vec{R}_J(t)|}, \tag{4}$$

where the instantaneous density $n(\vec{r},t)$ is given by the sum of all individual electronic orbitals, i.e.,

$$n(\vec{r},t) = \sum_{i=1}^{occ}|\varphi_i(\vec{r},t)|^2, \tag{5}$$

with $\varphi_i(\vec{r},t)$ being occupied orbital for the ith electron.

Similarly, to obtain $n(\vec{r},t)$ explicitly, instead of solving Eq. (1), we make use of the corresponding time-dependent density-functional theory with Kohn-Sham (KS) scheme,

which provides an exact description of $n(\vec{r},t)$,

$$i\frac{\partial\varphi_i(\vec{r},t)}{\partial t}=\left[-\frac{1}{2}\nabla^2-\sum_I\frac{Z_I}{|\vec{R}_I(t)-\vec{r}|}+\int\frac{n(\vec{r}',t)}{|\vec{r}-\vec{r}'|}d\vec{r}'+V_{xc}(\vec{r}',t)\right]\varphi_i(\vec{r},t), \quad (6)$$

where V_{xc} is the time-dependent exchange-correlation potential, which is initially a functional of the density $n(\vec{r}',t')$ at all points $\vec{r}'$ and at all times $t'<t$. Since the adiabatic approximation is exploited in this work, the memory effects of V_{xc} are not taken into account, V_{xc} is only a functional of $n(\vec{r}',t)$ at the current time t. The other three terms on the right-hand side of Eq. (6) are, in order, the electronic kinetic, the electron-nucleus potential, and the Hartree potential. The above Ehrenfest coupled electron-ion dynamics combined with time-dependent density-functional theory is known as ED-TDDFT. In the present work, only valence electrons of the projectile and host atoms ($1s$ for helium atom, $4sp$ for gallium, and $2sp$ for nitrogen) are explicitly included, the coupling of valence electrons to ionic cores is described by using norm-conserving Troullier-Martins (TM) pseudopotentials [39].

In ED-TDDFT, both the transitions between electronic adiabatic states and the coupling of adiabatic states with the nuclei trajectories are taken into accountant [40]. It thus allows *ab initio* molecular dynamics simulation for excited electronic states and makes possible the study of electron transfer between the projectile ion and the host atoms during the collision [41]. In this model, the potential energy and force acting upon the ions are calculated on the fly as the simulation proceeds. Note that ED-TDDFT only promises accuracy for the ion-to-electron energy transfer, the inverse process is poorly described [38]. However, such failure of Ehrenfest dynamics can only make very marginal effect to our results. Since the collision in the present work is completed within a few femtoseconds, much lower than the timescale of electron-phonon coupling that is picoseconds level [42].

The simulations were carried out by using the OCTOPUS *ab initio* real-space code [43,44] and employing the adiabatic local-density approximation with Perdew-Wang analytic parametrization [45] for the time-dependent exchange-correlation potential. There is no basis set in the present work, the external potential, electronic density, and KS orbitals are discretized in a set of mesh grid points with a uniform spacing of 0.18 Å along the three spatial coordinates in the simulation box. A small time step of 0.001 fs is adopted to ensure the stability of the time-dependent computations. Simulations with smaller time steps and grid spacings give essentially the same results.

The host crystalline thin film is isolate atom cluster, and no periodic boundary condition is employed in this work. At the initial stage of simulations, a ground-state DFT calculation is preformed to obtain the converged ground state of the host atom cluster. Then the intruding helium ion are channeled from a point 3 Å above the thin film with given descending velocities along the negative z direction. Ionic motion of target atoms is neglected by fixing the host ions in the equilibrium positions as they are expected to play only a marginal role under the well-channeling conditions [46]. Calculations with

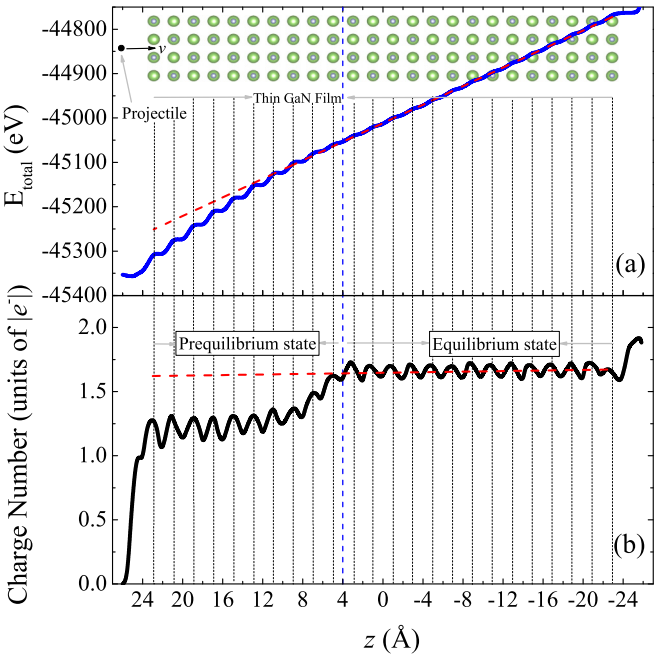

FIG. 1. (a) The evolution the total system energy when a helium ion with velocity of 0.36 a.u. is traversing the GaN thin film with thickness of 46 Å. The projectile ion moves from $z=23$ to -23 Å in the ⟨100⟩ channel along the main axis. (b) The number of induced charge when the ion is moving through the GaN thin film. The oscillations reflect the periodicity of the lattice. After the ion passing several lattice planes, it reaches charge equilibrium state. The vertical blue dashed line shows the position where the projectile reaches equilibrium state. The red dashed lines in (a) and (b) are linear fits to the total system energy and induced charge number after the ion reaches equilibrium state, respectively. The S_e is extracted from the slope of the fit to the total system energy after the ion reaches equilibrium state. The induced charge number in (b) is obtained by integrating the balance values between the perturbed and nonperturbed electron density in spheres with radius of 1.26 Å around the flying projectile. The inset shows the sketch of the crystal and projectile at the very beginning of the collision, the gray and green balls denote nitrogen nuclei and gallium nuclei, respectively.

relaxed host atoms will not significantly increase the amount of computation, but preserving strict translational symmetry of the atomic arrangement makes the Coulomb field exerted on the channeling ion by the lattice layers strictly periodic in time and space. The key quantity of interest S_e is extracted from the change of the total system energy over the distance after the projectile ions reach equilibrium states in the thin film.

Figure 1 presents position-resolved total system energy and the number of induced charge by a helium projectile moving through the calculation crystalline thin film. In the present work, the induced charge within a small region is deemed as the summation of instantaneous bound states charge captured by the initially bare projectile ion and the continuum states charge of the target attracted by the partially neutralized ion, it is obtained by integrating the balance values between the ground state and time-dependent calculation in a sphere with radius of 1.26 Å around the moving projectile. Such

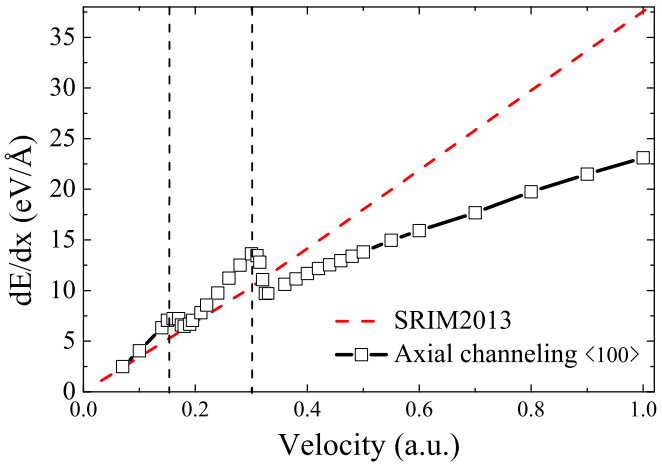

FIG. 2. Electronic stopping power (black open squares) for axially channeled helium ions as a function of velocity along ⟨100⟩ direction, together with the SRIM-2013 predictions (red dashed line). S_e shows local peaks at about 0.15 and 0.30 a.u.. The black solid line is drawn to guide the eye.

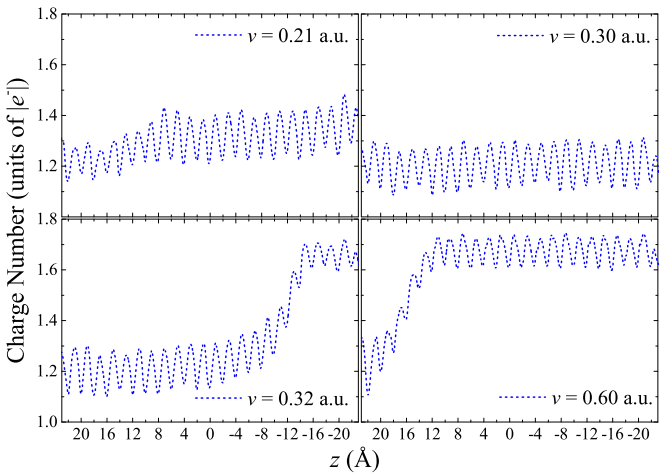

FIG. 3. The position-resolved induced charge of axially channeled helium ions with velocities of 0.21, 0.30, 0.32, and 0.6 a.u. along the trajectory in GaN thin film, respectively. The channeling ions move from $z = 23$ to -23 Å along the ⟨100⟩ direction. Except for $v = 0.3$ a.u., there are marked charge accumulations around the moving ions at initial stage, then the charge reach steady states after the ions travel certain distance.

integral radius is carefully chosen, and it is a tradeoff between computational accuracy and phenomenal sensitivity.

III. RESULTS AND DISCUSSION

A. Nonlinear S_e in ⟨100⟩ channel

We present in Fig. 2 the simulated S_e results for the motion of helium ions with velocity of 0.07–1.0 a.u. along the midaxis of ⟨100⟩ channel in GaN thin film. Also shown are the predictions from the SRIM-2013 database. The calculated data are extracted without the presence of preequilibrium contributions to the stopping of ions in conducting solids. To allow time for the intruding ion getting fully equilibrated during passage through the crystal, which may take several femtoseconds [47], a relatively thick $6\times6\times26$ Å^3 calculation box, containing a fcc-structured $2\times2\times12$ conventional cell comprising 192 Ga and 192 N atoms is employed. The lattice parameter exploited in this work is 3.985 Å.

As can be seen in Fig. 2, only qualitative agreement between the calculated results and the SRIM predictions can be achieved, which can be justified by the fact that, SRIM does not explicitly account for any special information of the channeling conditions studied in the present calculations, be it either the ordered lattice structure of the target material, or the local electronic structure [6,48]. The most striking feature of Fig. 2 is that S_e shows two distinctly different trends. Velocity proportionality is valid for relatively high-velocity regime ($v > 0.33$ a.u.). While for the velocity range below, local peaks appear at around $v = 0.15$ and 0.30 a.u., such character is obviously inconsistent with the velocity-proportionality assumption.

We have found through direct simulation that S_e responds readily to the charge state of the projectile, which has been reported to have a tremendous effect on the electronic energy loss [24,26,49]. In a simple intuitive picture: the screening charge around the ion keep it from rubbing the host electrons directly, which leads to a reduction of the Coulomb interaction between the projectile and the host electrons.

The position-resolved induced charge number by projectile ions are presented in Fig. 3. The ions move from $z = 23$ to -23 Å in the crystalline channel. As can be seen, it continues to oscillate with the changing atomic environment along the ion's path, after a passage of several atom planes, it does so around a mean value that depends on the ion's velocity. For projectile with velocity of 0.21 a.u., it reaches equilibrium state after traveling about 8 lattice atom planes at $z = 6$ Å. For projectile with velocity of 0.6 a.u., it reaches equilibrium state after penetrating about 6 lattice atom planes at $z = 12$ Å. For projectile with velocity of 0.32 a.u., which is close to the stopping peak at 0.30 a.u., equilibrium state is achieved after a passage of 18 lattice atom planes at $z = -14$ Å. While for projectile with velocity of 0.30 a.u., which is the velocity corresponding to a stopping peak, it seems the charge accumulation process is suppressed dramatically and no new equilibrium state accompanied by an increase of average induced charge is found. Basically, it is difficult to achieve charge equilibrium state with enhanced negative charge at or around the velocities corresponding to local stopping peak. The reason for such phenomenon shall be demonstrated in the following part.

In addition to the instantaneous induced charge, we also monitor the forces acting on the ions. Figure 4 presents the position-resolved forces along the movement direction on the channeling ions with different velocity. According to Eq. (4), it depends on pairwise repulsive forces and Hellmann-Feynman forces due to the electronic system. To show a more general trend, the average values of adjacent peaks and valleys are also presented. For projectile velocity at 0.3 a.u., which is the velocity corresponding to a local stopping peak, the average forces on the projectile almost keep constant. For projectiles with other velocities, the general trend is that, the

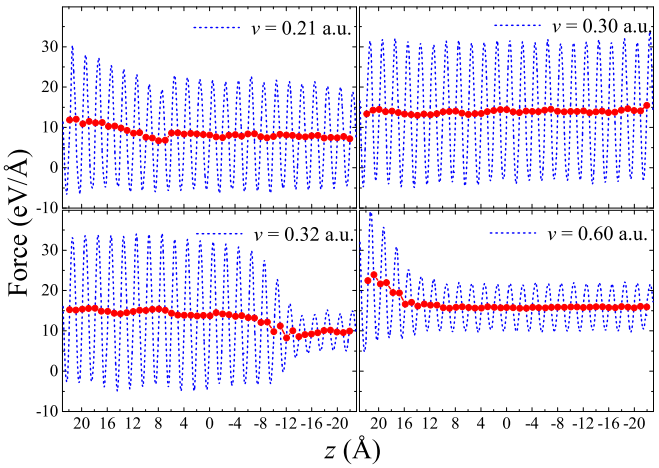

FIG. 4. The blue dashed lines show the instantaneous forces experienced by the axially channelled helium ion with different velocities along the motion direction. The red dots show the average values of adjacent peaks and valleys. The channeling ions move from $z = 23$ to -23 Å along the ⟨100⟩ direction. The red lines are drawn to guide the eye.

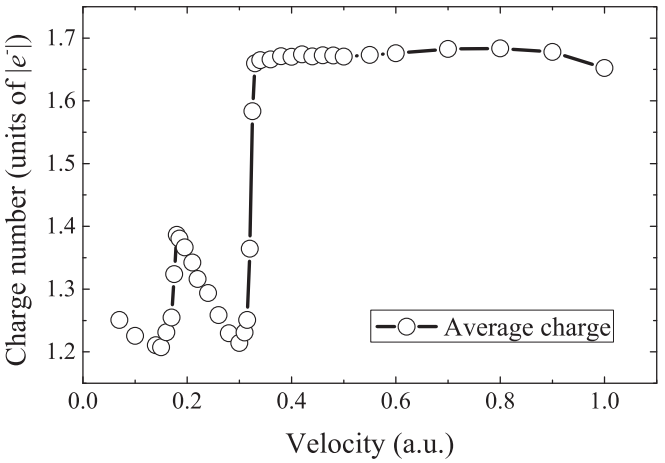

FIG. 5. Velocity-resolved average induced charge for axially channelled helium ions at steady states. See more details in the text. The line is drawn to guide the eye.

average forces keep falling until they reach steady states at certain points after the ions traveling several atom layers.

Another finding in Fig. 4 is that, due to the relatively low charge accumulation around the projectile at the initial stage of the channeling (as shown in Fig. 3), the average forces on the projectile increase with ion speed for the range of velocity considered, which is consistent with the prediction by FEG model [15]. The final average forces, however, are significantly affected by the charge accumulation. For instance, the final average force on 0.32 a.u. projectile is lower than that on 0.30 a.u. one, which is contrary to the prediction by the FEG model.

In general, the instantaneous forces demonstrated in Fig. 4 show an inverse trend with induced charge number presented in Fig. 3, and the two parameters reach steady values simultaneously. The average forces inserted on the projectile drop significantly as the induced charge increases, and the reduction of average induced charge is associated with an increase in the instantaneous force, indicating a direct correlation between the charge accumulation around the penetrating ion and the stopping.

In order to make sense the nonlinear S_e illustrated in Fig. 2, we demonstrate in Fig. 5 the effective charge of equilibrium states for projectiles with different velocity. These are nothing but the average values of induced charge over trajectories after they reach equilibrium states. Effective charge can be regarded as the average value around which the induced charge oscillates. Inverse traits between Figs. 2 and 5 in velocity regime below 0.33 a.u. can be found: there are valleys of effective charge at around 0.15 and 0.30 a.u., and two steep slopes follow closely the valleys. The effective charge reaches relative steady state at velocity regime above 0.33 a.u., and no nonlinear S_e occurs in this regime. The synchronous and inverse trend of effective charge and S_e suggests the nonlinear phenomenon at relatively low-velocity regime in Fig. 2 is caused by the odd effective charge behavior.

B. Resonant coherent excitation

The change of average induced charge in Fig. 5 indicates the change of bound charge states on the moving ions, its formation is accompanied by charge transfer, which is subject to a variety of mechanisms. In addition to the direct transitions such as excitation, ionization, and capture [50], the Auger process between the host atoms and ions also plays an important role, where an electron jumps from the valence band of the host atom to an ion bound state and vice versa. The energy released in such transition is balanced by an electronic excitation in the medium or on the projectile [51]. Another pronounced mechanism is the resonance process, in which an ion moving through the lattice feels a time-dependent potential with characteristic frequency depending on the ion velocity and lattice layer spacing, which may result in a transition of electron between the bound level of the ion and conduction band of the target [52,53].

The steep reduction of effective charge within a narrow window (e.g., around 0.3 a.u.) shown in Fig. 5 implies resonance excitation is of significance in this regime. Such process is associated with a net positive charging of the channeling ion, which keeps the initially bare projectile from reaching a equilibrium state with enhanced negative charge. The valleys of effective charge at around $v = 0.15$ and 0.3 a.u. in Fig. 5 are interpreted as results of the competition between the resonance excitation and other charge exchange processes. Moreover, the width of the resonance velocity regime is associated with the number of effective interactions with charge states on the penetrating ion.

The scenario describes that when swift atoms or ions are channeled through a crystal foil, they feel a superposition of periodic perturbation generated by a periodic lattice structure in the crystal. The influence of periodic perturbation on the electronic transitions can be quantitatively evaluated by the resonance energy $\hbar\omega$, where the resulting frequency is determined by the impact velocity and the spacing (denoted by d) between tetrahedral points in the channel, i.e., $\omega = 2k\pi|v|/d$, where k is an integer, v is the projectile velocity. When the energy difference between two electronic states,

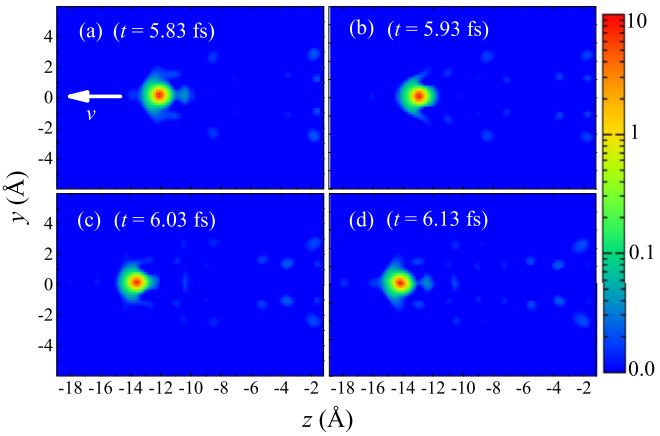

FIG. 6. One period of the charge oscillation for the channeling ion with velocity of 0.3 a.u.. The ion is traveling right to left along the main axis of ⟨100⟩ channel. (a) At $t = 5.83$ fs, the present distribution is generally a sphere; (b) at $t = 5.93$ fs, the shape of charge distribution has changed into ellipsoid; (c) at $t = 6.03$ fs, the shape of charge distribution is recovering to sphere; (d) at $t = 6.13$ fs, the shape of charge distribution has turned into sphere, and some charge have been left behind.

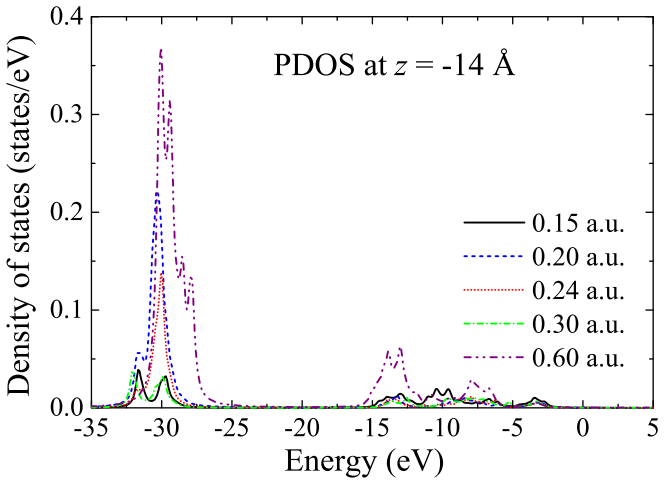

FIG. 7. The instantaneous PDOS on the projectiles with velocities of 0.15, 0.20, 0.24, 0.30, and 0.60 a.u., respectively, the Fermi energies are set to zero.

either both are on the channeling ion or one be the conduction band state of the host medium, matches with one of resulting frequencies, the ionic charge is resonant-coherently excited. Such a resonant excitation is referred to as resonant coherent excitation (RCE) [54]. This process depends both on the energy states of the projectile and on discrete periodic nature of the atomic lattice. Thus, RCE can occur only when the quantum character of the electrons and the atomic structure of the host lattice are treated explicitly.

Due to the space-periodic potential from lattice atoms, the induced charge distribution around a channeling ion is different from the description in linear response models [16,55,56] that the induced charges lag behind the projectile and form the wake potential. In this work, the screening charges around the penetrating ion are found to keep oscillating back and front when it is moving along the ⟨100⟩ midaxis of the zinc-blende crystalline GaN.

We present in Fig. 6 the snapshots of charge oscillation process for helium ion penetrating a host cluster with 384 atoms. At $t = 5.83$ fs, the projectile in Fig. 6(a) moves and squeezes the electrons in the front, which looks like the image of a flying bullet shoving the air, the present screening charge distribution is generally spherical. Shortly thereafter, at $t = 5.93$ fs, the charge distribution shown in Fig. 6(b) around the projectile has been pulled into an ellipsoid by the potential from lattice atoms. Subsequently, when the time comes to $t = 6.03$ fs, the charge distribution in Fig. 6(c) begins to recover. Eventually, at $t = 6.13$ fs, the charge distribution in Fig. 6(d) has returned to sphere and some charge has been left behind. The charge oscillation period for $v = 0.3$ a.u. is 0.30 fs, equaling to the time for the projectile flying through a periodic repeat distance, which verifies the existence of space-periodic potential from lattice atoms.

In order to demonstrate the effect of resonance excitation on the bound states charge of the projectile more directly, we calculate the projected density of states (PDOS) on the $1s$ orbital of the projectile. To show the derivation completely, we also give the definition of the density of states (DOS)

$$\rho(\varepsilon) = \sum_{i}^{occ} \langle\varphi_i|\varphi_i\rangle\delta(\varepsilon - \varepsilon_i), \tag{7}$$

where ε_i is the eigenvalue of the eigenstate φ_i. Inserting a complete orthonormal basis,

$$1 = \sum_{j} |j\rangle\langle j|, \tag{8}$$

this can be rewritten as

$$\rho(\varepsilon) = \sum_{j} \rho_j(\varepsilon), \tag{9}$$

where $\rho_j(\varepsilon)$ is the PDOS on the j orbital, with

$$\rho_j(\varepsilon) = \sum_{i} \langle\varphi_i|j\rangle\langle j|\varphi_i\rangle\delta(\varepsilon - \varepsilon_i). \tag{10}$$

Energy integrating of the PDOS below Fermi energy multiplied by a occupation number per state gives the number of bound electrons on the j orbital of the projectile.

Given that PDOS calculation is very computation consuming, we performed such calculations in a $2\times2\times8$ conventional cell with 256 host atoms, much smaller than the one used in the above subsection with 384 host atoms. The PDOS on projectile with different velocities at $z = -14$ Å are demonstrated in Fig. 7. The ions move from $z = 15$ to -15 Å along ⟨100⟩ main axis in the crystalline channel. As can be seen the amplitudes of the PDOS for $v = 0.15$ and 0.30 a.u. are dramatically lower than that of the other velocities. The result shows that due to the effect of RCE, the number of bound states charge on the projectile is greatly suppressed.

We also integrate the PDOS of the $1s$ state of projectile over energy below Fermi energy to obtain the charge captured to the bound states of the projectile, which is the balance of RCE and other charge transfer processes. Figure 8 presents the change of the bound states charge on projectile with different

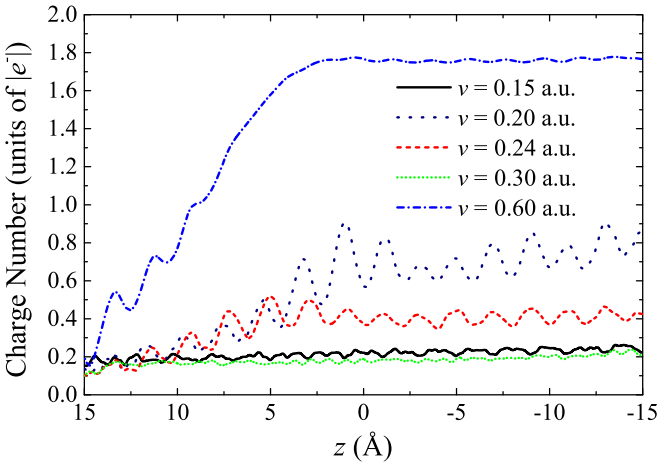

FIG. 8. The position-resolved bound states charge captured by the projectile obtained by integrating the PODS on the He-1*s* state of the projectiles with velocities of 0.15, 0.20, 0.24, 0.30, and 0.60 a.u., respectively.

velocities along the trajectory of ⟨100⟩ main axis. Consistent with the character of PDOS, the amplitudes of the bound states charge for $v = 0.15$ and 0.30 a.u. are significantly lower than that of the other velocities. A common feature for $v = 0.20$, 0.24, and 0.6 a.u. is that the drastic charge capture and loss process occurs alternatively until the projectiles reach charge equilibrium states. The difference is that, the charge capture and loss behavior of the projectile after it reach charge equilibrium state is relatively mild for $v = 0.60$ a.u., while it is quite intense for $v = 0.20$ and 0.24 a.u.. Such result can be interpreted as a consequence of longer interaction time with neighboring host atoms for projectiles with lower velocities.

To demonstrate the velocity-resolved electronic screening by bound states charge on the projectile, we present in Fig. 9

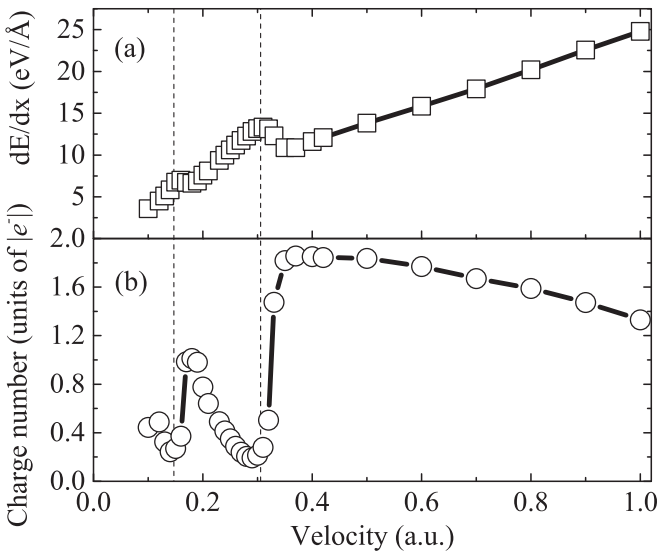

FIG. 9. (a) Electronic stopping power for helium moves in cluster with 256 atoms. (b) Velocity-resolved average captured charge for axially channelled helium ions at steady states. See more details in the text. The lines are drawn to guide the eye.

the average charge captured by the projectiles over the last 4 Å ionic range in crystal, i.e., from $z = -11$ to $z = -15$ Å. For comparison, the corresponding electronic stopping power is also demonstrated. Similar trend of bound states charge versus velocity with the induced charge shown in Fig. 5 is found, there are valleys for the bound states charge at $v = 0.15$ and 0.30 a.u.. However, the amplitude of bound states charge is much lower than that of induced charge in the valley, suggesting considerable number of target continuum states charges are polarized around the highly stripped ions. It is to be noted that, although the bound states charge relative with the RCE more directly, both the screening effects by the captured charge and by the target continuum states charge contribute to the electronic stopping, since the calculations of Hellman-Feynman force in Eq. (4) do not distinguish between an electron belonging to the projectile or target atoms. The induced charge (both electrons captured or just attracted by the projectile) is more suitable to reflect the screening effect on the projectile nucleus, instead of just the bound states charge, which can also be inferred by the fact that the velocities corresponding to minimum value of bound states charge and the maximum value of the stopping power are not fully overlap in Fig. 9.

Similar resonance phenomenon was reported by Mason and Race *et al.* [19,34]. Using time-dependent tight-binding model, they observed a resonant charging phenomenon in the valence electron states for self-irradiated copper, and they found an enhancement of negative charge on the channeling ion for projectiles at narrow velocity window. Such result was interpreted as a consequence of the resonant excitation of electrons in delocalized states near the Fermi energy onto the defect states highly localized on the channeling ion during passage through the host matter. This conclusion was also verified by their DFT calculation, where a sharp peak for the local DOS on the projectile above Fermi energy was found. In present work, similar phenomenon is reproduced. We find DOS peaks of the ion-solid system above Fermi energy for projectiles traveling with velocity $0.2 \leqslant v \leqslant 0.37$ a.u.. Such velocity regime just corresponds to the charge valley in Fig. 9, which suggests the peaks of DOS above Fermi energy in present work are also caused by resonant excitations. The DOS of the ion solid for projectile with velocity of 0.21, 0.30, 0.35, and 0.37 a.u. at $z = -14$ Å is presented in Fig. 10, the bulk GaN DOS are also shown for comparison. For $v = 0.21$ a.u. and $v = 0.35$ a.u., the resonance peak appears at around $E = 3$ eV. The amplitude of resonance peak reaches its maximum at $v = 0.30$ a.u.. For $v = 0.37$ a.u., i.e., the very edge of the charge valley in Fig. 9, the amplitude of resonance peak almost disappears. The amplitude of resonance peak reflects the strength of the resonance, and the trend of which is in consistent with the velocity-resolved captured charge valley shown in Fig. 9.

The different charge change at resonance velocity window in Mason and Race's work and the present work resides in the specific electronic structures. There are unoccupied states lying above the Fermi energy on the projectile in their work, which leads to an enhancement in negative charge when the resonance happens. While, in the present work, the PDOS on the projectile completely lies below Fermi energy, the resonance mainly results in an excitation of charge from

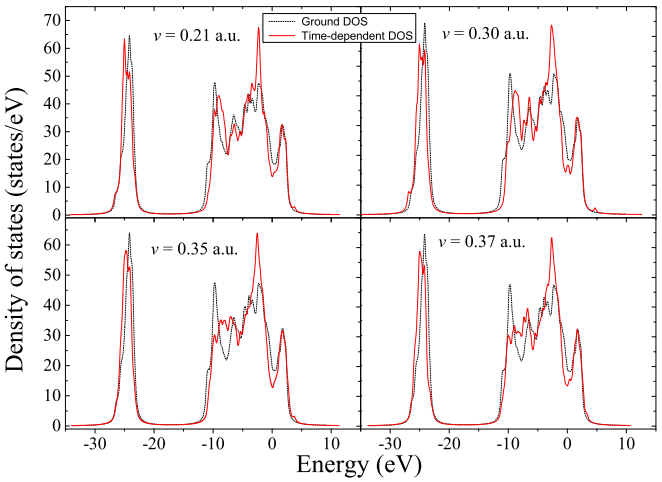

FIG. 10. The density of states of the ion solid for projectile with velocity of 0.21, 0.30, 0.35, and 0.37 a.u. at $z = -14$ Å, the Fermi energies are set to zero. The bulk GaN density of states is also shown for comparison, the amplitude of the resonance peaks appear with varied degrees for different velocities. Such calculations are performed with the host cluster including 256 atoms, The ions move from $z = 15$ to -15 Å along ⟨100⟩ main axis in the crystalline channel. See text for more information.

occupied states of the projectile onto the conduction band of the ion-solid system, accompanying by a depletion in the negative charge on the projectile.

C. Direction dependence of resonant coherent excitation

In order to make a further exploration of space-periodic potential by an array of the atomic planes, we investigate the S_e and effective charge of helium ion moving along the main axis of ⟨110⟩ channel, for which the distance between lattice planes along the ion trajectory is different from that of ⟨100⟩ channel. An off-center channeling parallel to ⟨100⟩ axis is also investigated.

Figure 11 presents the S_e and average induced charge of helium ion implanted along the main axis of ⟨110⟩ channel. It demonstrates in Fig. 11(a) a qualitatively similar behavior as the axial channeling along the ⟨100⟩ direction, the nonlinear S_e in low-velocity regime also appears, there are local peaks at about $v = 0.22$ and 0.44 a.u., respectively. The effective charge in Fig. 11(b) also shows local valleys at around $v = 0.22$ and 0.44 a.u., which additionally reflects the S_e has a direct relation with effective charge, and 0.22 and 0.44 a.u. are characteristic velocities of RCE that excite the ionic charge effectively under ⟨110⟩ axial-channeling condition. It is noteworthy that the velocities corresponding to S_e peaks in ⟨110⟩ channel are about $\sqrt{2}$ times of the velocities in ⟨100⟩ channel, the ratio of the spacing along ⟨110⟩ row and ⟨100⟩ row is also $\sqrt{2}$, which furthermore suggests the existence of the aforementioned quantitative space-periodic potential.

We present in Figs. 12, the S_e and effective charge of helium ion implanted along a trajectory parallel to ⟨100⟩ axis with $a/8$ (a denotes lattice parameter) displacement from channel center, respectively. As can be seen, valley of the average induced charge is found only at about $v = 0.15$ a.u..

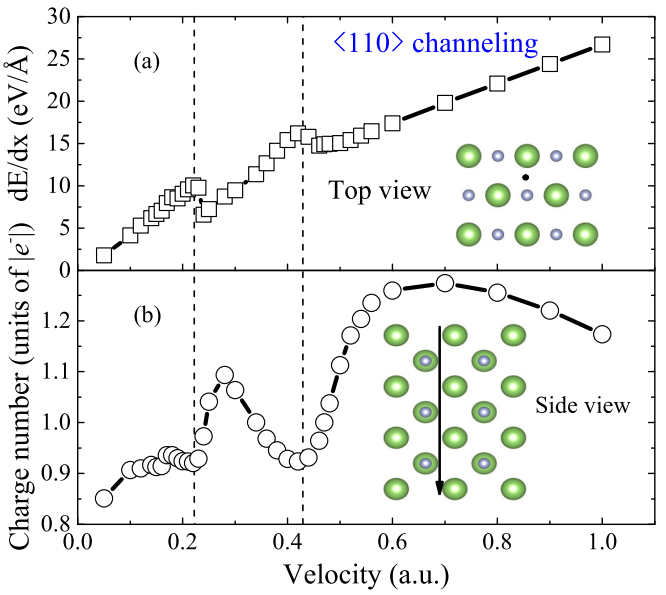

FIG. 11. The S_e (a) and effective charge (b) of helium ion traveling along the midaxis of ⟨110⟩ channel. The black lines are drawn to guide the eye. The vertical dashed lines at $v = 0.22$ and 0.44 a.u. show the velocities at which the local peaks of S_e and the local valleys of effective charge occur. The black dot in penal (a) shows the top view of the projectile ion trajectory, the black arrow line in (b) shows the side view of the projectile ion trajectory.

According to the interpretations in Ref. [54], lowering the impact parameter would increase charge capture cross sections. Projectile ions, which have been coherently excited and ionized will immediately capture an electron and rejoin the

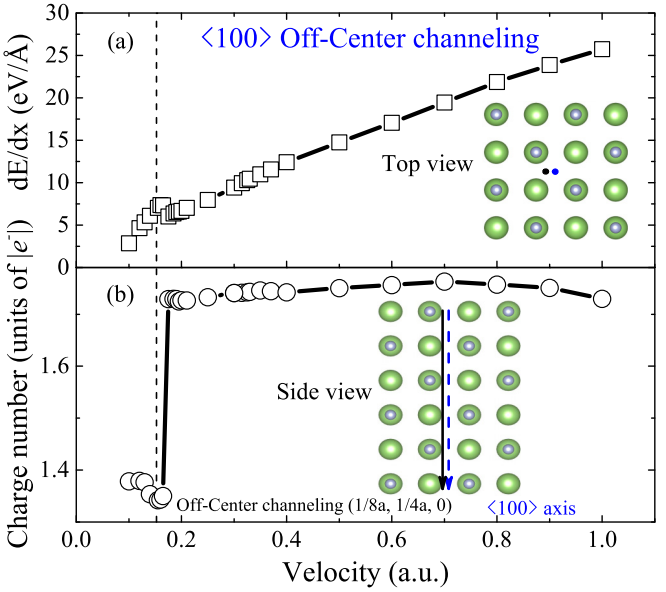

FIG. 12. The S_e (a) and effective charge (b) of helium ion implanted along the ⟨100⟩ direction with $a/8$ displacement in x direction from main axis. The black lines are drawn to guide the eye. The blue dashed arrow line and the black solid arrow line in inset of (b) denote the ⟨100⟩ axis and the ion trajectory of the off-center channeling, respectively.

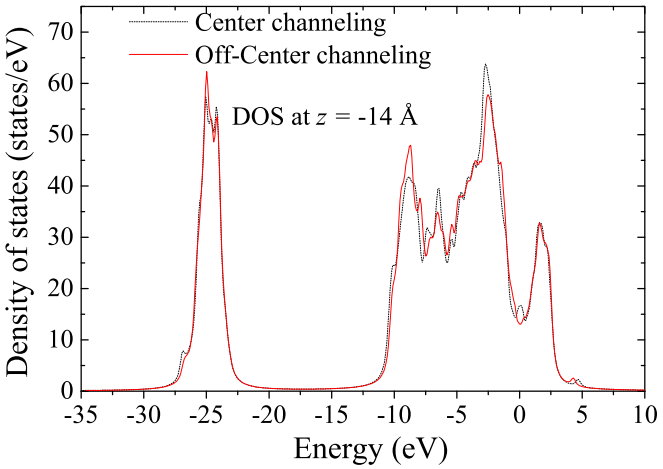

FIG. 13. The instantaneous DOS of ion-solid for projectile with velocity of 0.30 a.u. at $z = 14$ Å for the center channeling and off-center channeling cases respectively, the Fermi energy is set to zero. Such calculations are performed with the host cluster including 256 atoms. The ions move from $z = 15$ to -15 Å along ⟨100⟩ main axis in the crystalline channel.

equilibrium states. Especially for projectile with high velocity, more free conducting electrons are available to be captured due to the greater perturbation to the host atoms.

In order to verify the above statement, we present in Figs. 13 and 14 the DOS of ion solid and the PDOS on the 1s state of the projectile for off-center channeling trajectory with velocity of 0.3 a.u., respectively, the corresponding plots for projectile moving along the ⟨100⟩ axis are also shown for comparison. As can be seen, the resonance peak at conduction band also appears for the off-center channeling at around $E = 4.3$ eV, which means there is RCE in such condition. However, the amplitude of the PDOS for off-center channeling is much higher than that of center channeling, suggesting other capture and loss processes are dominant under the off-center channeling condition, and the effect of RCE is concealed.

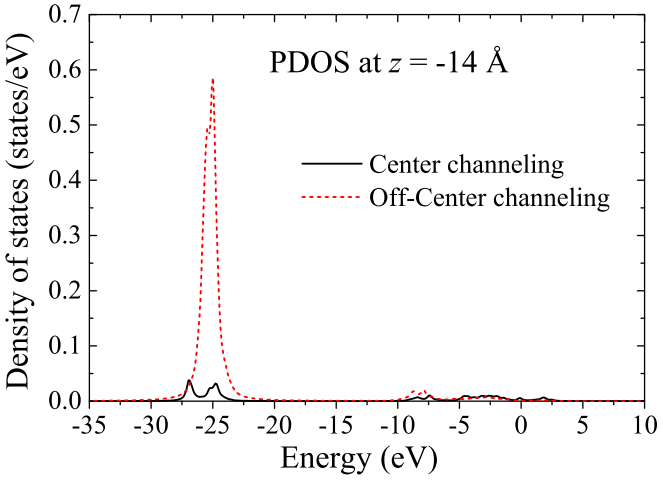

FIG. 14. The instantaneous PDOS on the 1s state of helium projectile with velocity of 0.30 a.u. at $z = 14$ Å for the center channeling and off-center channeling cases, respectively, the Fermi energy is set to zero. Such calculations are performed with the host cluster including 256 atoms. The ions move from $z = 15$ to -15 Å along ⟨100⟩ main axis in the crystalline channel.

IV. CONCLUSIONS

We report theoretical study from first principles the nonadiabatic interaction of slow helium ions with zinc-blende GaN cluster under channeling conditions. It is found electronic energy loss is quite sensitive to charge states of the projectile. Our TDDFT calculations show that the periodic lattice atoms have a nontrivial influence on the effective charge of the low-velocity projectile through RCE at narrow windows, which furthermore results in the change of the slope for electronic stopping versus velocity. We have also shown the charge oscillation of the channeling ion and the direction dependence of RCE.

Our work has unveiled one of the most fundamental consequences of the nonadiabaticity of the channeling interaction of ion solid. RCE is expected to be of significance in evaluating the stopping of slow heavy ions channeling interaction problems. The direction dependence of RCE and the resulting charge oscillation indicates the nonlinear stopping in this work is in correlation with the lattice atom distribution, which is beyond the frame of free electron gas and linear response approximations that treat the electronic structure of lattice atom implicitly. We have also found such RCE phenomenon in other crystals with Fm-3m group structure, such as TiN, AlN, and MgO. A common feature for these crystals including the GaN in the present work and Cu in Mason and Race's works [19,34] is that the layers of the lattice are highly translational symmetric. The corresponding results will be released in our future work.

As far as we know, prior works about RCE are mainly focus on the high-energy regime corresponding to core electron transition, which mainly results in the excitation of inner-shell electron on the projectile, both the excitations and deexcitations process are relevant. In the present work, effect of RCE mainly resides in the excitation of valence charge from the projectile charge to the conduction band of target continuum states. The deexcitations may only be of minor significance, so our results are not adversely affected by the fact that Ehrenfest dynamics falls to handle spontaneous phonon emission. We hope this work may stimulate further experimental and theoretical work on resonant coherent excitation of the valence charge on the projectile with low velocity.

ACKNOWLEDGMENTS

This work was supported by the National Natural Science Foundation of China under Grants No. 51727901, No. 11635003, No. 11025524, and No. 11161130520, National Basic Research Program of China under Grant No. 2010CB832903, the European Commissions 7th Framework Programme (FP7-PEOPLE-2010-IRSES) under Grant Agreement Project No. 269131 and Beijing Natural Science Foundation No. 2192049. The numerical calculations in this paper have been done on the supercomputing system in the Supercomputing Center of Wuhan University.

[1] H. Bethe, Ann. Phys. (NY) **397**, 325 (1930).
[2] F. Bloch, Ann. Phys. (NY) **408**, 285 (1933).
[3] P. Sigmund, Phys. Rev. A **56**, 3781 (1997).
[4] D. Primetzhofer, Phys. Rev. B **86**, 094102 (2012).
[5] K. G. Reeves, Y. Yao, and Y. Kanai, Phys. Rev. B **94**, 041108(R) (2016).
[6] E. E. Quashie, B. C. Saha, and A. A. Correa, Phys. Rev. B **94**, 155403 (2016).
[7] A. Blažević, H. G. Bohlen, and W. von Oertzen, Phys. Rev. A **61**, 032901 (2000).
[8] C. L. Zhang, X. H. Hong, F. Wang, Y. Wu, and J. G. Wang, Phys. Rev. A **87**, 032711 (2013).
[9] E. A. García, N. P. Wang, R. C. Monreal, and E. C. Goldberg, Phys. Rev. B **67**, 205426 (2003).
[10] R. A. Wilhelm, E. Gruber, J. Schwestka, R. Kozubek, T. I. Madeira, J. P. Marques, J. Kobus, A. V. Krasheninnikov, M. Schleberger, and F. Aumayr, Phys. Rev. Lett. **119**, 103401 (2017).
[11] D. Primetzhofer, S. Rund, D. Roth, D. Goebl, and P. Bauer, Phys. Rev. Lett. **107**, 163201 (2011).
[12] D. Primetzhofer, Phys. Rev. A **89**, 032711 (2014).
[13] R. Cabrera-Trujillo, P. Apell, J. Oddershede, and J. R. Sabin, in *17th International Conference on the Application of Accelerators in Research and Industry*, edited by J. L. Duggan, I. L. Morgan, and M. Hall, AIP Conf. Proc. No. 680 (AIP, New York, 2003), p. 86.
[14] A. Mertens and H. Winter, Phys. Rev. Lett. **85**, 2825 (2000).
[15] E. Fermi and E. Teller, Phys. Rev. **72**, 399 (1947).
[16] R. H. Ritchie, Phys. Rev. **114**, 644 (1959).
[17] D. Roth, B. Bruckner, M. V. Moro, S. Gruber, D. Goebl, J. I. Juaristi, M. Alducin, R. Steinberger, J. Duchoslav, D. Primetzhofer, and P. Bauer, Phys. Rev. Lett. **118**, 103401 (2017).
[18] J. F. Janni, At. Data Nucl. Data Tables **27**, 341 (1982).
[19] D. R. Mason, C. P. Race, M. H. F. Foo, A. P. Horsfield, W. M. C. Foulkes, and A. P. Sutton, New J. Phys. **14**, 073009 (2012).
[20] S. Datz, C. D. Moak, O. H. Crawford, H. F. Krause, P. F. Dittner, J. Gomez del Campo, J. A. Biggerstaff, P. D. Miller, P. Hvelplund, and H. Knudsen, Phys. Rev. Lett. **40**, 843 (1978).
[21] V. V. Okorokov, Yad. Fiz. **2**, 1009 (1965).
[22] V. V. Okorokov, JETP Lett. **2**, 111 (1965).
[23] S. Shindo and Y. H. Ohtsuki, Phys. Rev. B **14**, 3929 (1976).
[24] W. Brandt and M. Kitagawa, Phys. Rev. B **25**, 5631 (1982).
[25] S. D. Bloom and G. D. Sauter, Phys. Rev. Lett. **26**, 607 (1971).
[26] G. D. Sauter and S. D. Bloom, Phys. Rev. B **6**, 699 (1972).
[27] N. Bohr, Phys. Rev. **58**, 654 (1940).
[28] N. Bohr and J. Lindhard, K. Dan. Vidensk. Selsk. Mat.-Fys. Medd. **28**, No. 7 (1954).
[29] P. Echenique, R. Nieminen, and R. Ritchie, Solid State Commun. **37**, 779 (1981).
[30] P. M. Echenique, R. M. Nieminen, J. C. Ashley, and R. H. Ritchie, Phys. Rev. A **33**, 897 (1986).
[31] R. Ullah, F. Corsetti, D. Sánchez-Portal, and E. Artacho, Phys. Rev. B **91**, 125203 (2015).
[32] F. Mao, C. Zhang, J. Dai, and F.-S. Zhang, Phys. Rev. A **89**, 022707 (2014).
[33] M. Caro, A. Tamm, A. Correa, and A. Caro, J. Nucl. Mater. **507**, 258 (2018).
[34] C. P. Race, D. R. Mason, M. H. F. Foo, W. M. C. Foulkes, A. P. Horsfield, and A. P. Sutton, J. Phys.: Condens. Matter **25**, 125501 (2013).
[35] M. A. Zeb, J. Kohanoff, D. Sánchez-Portal, A. Arnau, J. I. Juaristi, and E. Artacho, Phys. Rev. Lett. **108**, 225504 (2012).
[36] F. Calvayrac, P. G. Reinhard, E. Suraud, and C. A. Ullrich, Phys. Rep. **337**, 493 (2000).
[37] J. L. Alonso, X. Andrade, P. Echenique, F. Falceto, D. Prada-Gracia, and A. Rubio, Phys. Rev. Lett. **101**, 096403 (2008).
[38] J. le Page, D. R. Mason, and W. M. C. Foulkes, J. Phys.: Condens. Matter **20**, 125212 (2008).
[39] N. Troullier and J. L. Martins, Phys. Rev. B **43**, 1993 (1991).
[40] X. Andrade, A. Castro, D. Zueco, J. L. Alonso, P. Echenique, F. Falceto, and A. Rubio, J. Chem. Theory Comput. **5**, 728 (2009).
[41] G. Avendaño-Franco, B. Piraux, M. Grüning, and X. Gonze, Theore. Chem. Acc. **131**, 1289 (2012).
[42] J.-H. Klein-Wiele, P. Simon, and H.-G. Rubahn, Phys. Rev. Lett. **80**, 45 (1998).
[43] M. A. L. Marques, A. Castro, G. F. Bertsch, and A. Rubio, Comput. Phys. Commun. **151**, 60 (2003).
[44] A. Castro, H. Appel, M. Oliveira, C. A. Rozzi, X. Andrade, F. Lorenzen, M. A. L. Marques, E. K. U. Gross, and A. Rubio, Phys. Status Solidi B **243**, 2465 (2006).
[45] J. P. Perdew and Y. Wang, Phys. Rev. B **45**, 13244 (1992).
[46] A. A. Correa, J. Kohanoff, E. Artacho, D. Sánchez-Portal, and A. Caro, Phys. Rev. Lett. **108**, 213201 (2012).
[47] M. Hattass, T. Schenkel, A. V. Hamza, A. V. Barnes, M. W. Newman, J. W. McDonald, T. R. Niedermayr, G. A. Machicoane, and D. H. Schneider, Phys. Rev. Lett. **82**, 4795 (1999).
[48] A. Schleife, Y. Kanai, and A. A. Correa, Phys. Rev. B **91**, 014306 (2015).
[49] J. I. Juaristi, A. Arnau, P. M. Echenique, C. Auth, and H. Winter, Phys. Rev. Lett. **82**, 1048 (1999).
[50] G. Schiwietz and P. L. Grande, Phys. Rev. A **84**, 052703 (2011).
[51] R. D. Muiño, Nucl. Instrum. Meth. B **203**, 8 (2003).
[52] A. Arnau, M. Peñalba, P. M. Echenique, and F. Flores, Nucl. Instrum. Meth. B **69**, 102 (1992).
[53] A. Arnau, M. Peñalba, P. M. Echenique, F. Flores, and R. H. Ritchie, Phys. Rev. Lett. **65**, 1024 (1990).
[54] C. D. Moak, S. Datz, O. H. Crawford, H. F. Krause, P. F. Dittner, J. Gomez del Campo, J. A. Biggerstaff, P. D. Miller, P. Hvelplund, and H. Knudsen, Phys. Rev. A **19**, 977 (1979).
[55] J. Lindhard, Dan. Vid. Selsk Mat.-Fys. Medd. **28**, 8 (1954).
[56] P. Echenique, F. Flores, and R. Ritchie, *Dynamic Screening of Ions in Condensed Matter* (Academic Press, New York, 1990), pp. 229–308.